This document is the Accepted Manuscript version of a Published Work that appeared in final form in ACS Applied Materials and Interfaces, copyright © American Chemical Society after peer review and technical editing by the publisher. To access the final edited and published work see: https://dx.doi.org/10.1021/acsami.8b09203.

Pentacene/TiO_2 anatase hybrid interface study by scanning probe microscopy and first principles calculations

Milica Todorović,[†,‡] Oleksandr Stetsovych,[¶,⊥] César Moreno,[§,#] Tomoko K. Shimizu,[¶,‖] Óscar Custance,[*,¶] and Rubén Pérez[*,†,@]

†*Departamento de Física Teórica de la Materia Condensada, Universidad Autónoma de Madrid, E-28049 Madrid, Spain*

‡*Department of Applied Physics, Aalto University, P.O. Box 11100, Aalto FI-00076, Finland*

¶*National Institute for Materials Science (NIMS), 1-2-1 Sengen, 305-0047 Tsukuba, Japan*

§*International Center for Young Scientists, NIMS, 1-2-1 Sengen, 305-0047 Tsukuba, Japan*

‖*Dept. Applied Physics and Physico-Informatics, Keio University, 3141 Hiyoshi, Yokohama, Kanagawa 223-8522, Japan*

⊥*Acad Sci Czech Republic, Inst Phys, Cukrovarnicka 10, Prague 16200 6, Czech Republic*

#*Catalan Institute of Nanoscience and Nanotechnology (ICN2), CSIC and The Barcelona Institute of Science and Technology, Campus UAB, Bellaterra, 08193 Barcelona, Spain*

@*Condensed Matter Physics Center (IFIMAC), Universidad Autónoma de Madrid, E-28049 Madrid, Spain*

E-mail: custance.oscar@nims.go.jp; ruben.perez@uam.es

Abstract

The understanding and control of the buried interface between functional materials in optoelectronic devices is key to improving device performance. We combined atomic resolution scanning probe microscopy with first principles calculations to characterize the technologically relevant organic/inorganic interface structure between pentacene molecules and the TiO_2 anatase (101) surface. A multipass AFM imaging technique overcomes the technical challenge of imaging simultaneously the corrugated anatase substrate, molecular adsorbates, monolayers and bilayers at the same level of detail. Submolecular resolution images revealed the orientation of the adsorbates with respect to the substrate and allowed direct insight into interface formation. Pentacene molecules were found to physisorb parallel to the anatase substrate in the first contact layer, passivating the surface and promoting bulk-like growth in further organic layers. While molecular electronic states were not significantly hybridized by the substrate, simulations predicted localized pathways for molecule-surface charge injection. The localized states were associated with the molecular LUMO inside the oxide conduction band, pointing to efficient transfer of photo-induced electron charge carriers across this interface in prospective photovoltaic devices. In uncovering the atomic arrangement and favorable electronic properties of the pentacene/anatase interface, our findings testify to the maturity and analytic power of our methodology in further studies of organic/inorganic interfaces.

Keywords: hybrid organic/inorganic interfaces, pentacene, anatase, AFM, DFT, thin film morphology

Introduction

Organic photovoltaic (OPV) devices, where thin films of organic molecules coated with metal oxide buffers are layered between metallic electrodes, provide an affordable route to manufacturing large-area, lightweight solar cells for universal use. Device operation is enhanced by

efficient electron-hole pair (exciton) separation into carrier charges in the organic region and directional intra-layer charge mobility. Favorable band alignment at the organic/inorganic interface is particularly important for effective charge injection across the layers, whereas poor contact between the two materials leads to carrier scattering and recombination that degrade device performance. All these factors depend on the electronic structure of the buried interface; by controlling it we can enhance the power conversion efficiency of OPV devices.[1]

Identifying the atomic arrangement at the organic/inorganic interface is critical to determining the local electronic band alignment. Atomic details of the interface structure are difficult to establish experimentally, so computational techniques are frequently deployed to simulate various molecule-solid contact configurations. Such calculations are made challenging by the large numbers of atoms and degrees of freedom involved; chemical intuition helps to identify relevant configurations, but without experimental verification there is no guarantee that the computed interface structure resembles the one in the actual device.

In this work, we pursue a combined theoretical and experimental approach to interface structure determination. A metal oxide surface was functionalised by organic molecules at varying degrees of coverage. TiO_2 anatase served as the prototype model oxide buffer material on account of its optical activity and high charge carrier mobility.[2,3] The (101) facet of an anatase natural crystal was covered with photoactive pentacene molecules; this is an electron acceptor molecule widely employed in organic optoelectronics.[4,5] These two materials play significant roles in the recent revival of dye-sensitized solar cells,[6,7] TiO_2 as substrate[8–10] and pentacene as a candidate for metal-free dyes,[11,12] which makes their interface a topic of current scientific interest.

Scanning probe microscopy (SPM), atomic force microscopy (AFM)[13] in particular, can now

achieve outstanding sub-molecular imaging of molecules on flat surfaces.[14,15] Structural detail is delivered by constant-height close-range scanning techniques with chemically inert CO-functionalized probes.[16] The considerable substrate corrugation of reconstructed metal oxide surfaces or large adsorbates presents a challenge for this imaging method, making it difficult to functionalize the probe with a CO molecule using vertical manipulation techniques or to scan the surface at constant height. To overcome this obstacle we opt for a 'multipass' imaging method. Developed to address high-resolution AFM imaging of large molecules on corrugated substrates, it allows us to obtain atomic-scale resolution detail of both surface and adsorbate simultaneously.[17]

Experimental characterization was carried out by combining 'multipass' AFM with bias spectroscopy imaging[18] and scanning tunnelling microscopy (STM).[19] In multi-channel measurements, probe-surface force and tunneling current signals were recorded simultaneously to obtain real-space local information on the chemical and electrical response of the functionalized surface. We employed first-principles density functional theory methods to interpret the contrast formation mechanisms behind AFM and STM imaging, and analyze the electronic properties at the surface. Such a comprehensive approach allowed us to study local bonding of the molecules to the crystal substrate, monolayer formation and thin film morphology, and thus reconstruct the typical interface structure. A similar approach may be employed to characterize the assembly and growth of complex surface nanostructures.

Results and Discussion

The wide area AFM scan of pentacene-covered TiO_2 anatase surface shown in Fig. 1(a) features a trapezoidal island typical of the (101) facet morphology.[20] Pentacene molecules adsorbed onto the island's terrace are distinguishable as bright, oblong objects. Sub-molecular

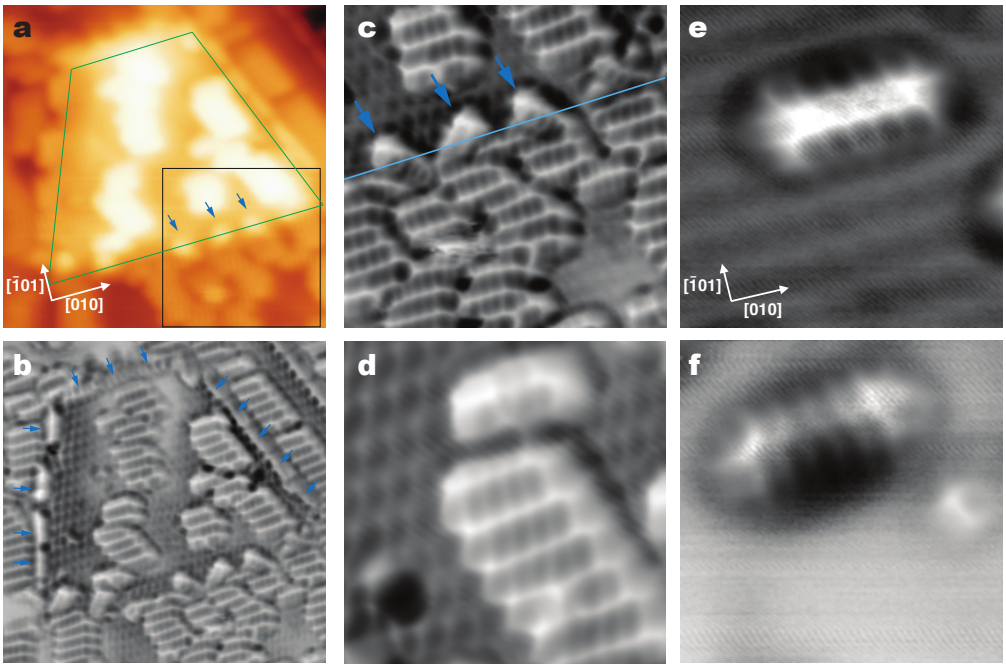

Figure 1: (a) Topographic AFM image of an area of (101) TiO_2 anatase partially covered with pentacene molecules(20×20 nm^2). Crystallographic orientation is the same in all images. The trapezoid highlights the contour of an anatase island. (b) Intramolecular resolution AFM image simultaneously acquired with the topography displayed in (a) showing details of the adsorption of pentacene molecules at the terraces and steps of the anatase surface (20×20 nm^2). The arrows point to pentacene molecules adsorbed at the steps in a side-on configuration. (c) Details of the adsorption of pentacene molecules (blue arrows) on the energetically most stable step of this anatase surface, connecting both upper and lower terrace (8.0×8.0 nm^2). The line indicate the position of the step edge as characterized from the topography. (d) Details of a stack of pentacene molecules simultaneously resolving atomic features of the (101) anatase surface (4.7×4.7 nm^2). (e) and (f) Frequency shift images of single pentacene molecules obtained with two different probe terminations (3.0×3.0 nm^2). Acquisition parameters are: free-oscillation first longitudinal resonant frequency (fo) of the cantilever was 152471 Hz for (a) to (d), and 159202 Hz for (e) and (f); cantilever oscillation amplitude (A) was 95.9 Å for (a) to (d), 169.1 Å for (e), and 135.3 Å for (f); cantilever stiffness (K) was 23.7 N/m for (a) to (d), and 26.9 N/m for (e) and (f); quality factor of the cantilever (Q) was 44163 for (a) to (d), 49188 for (e) and 44246 for (f). Topographic set point (Δf) was -3.0 Hz for (a) to (c), -4.0 Hz for (d), -4.5 Hz for (e) and -14.2 Hz for (f); approach distance towards the surface for sub-molecular imaging (d) was 300 pm for (b), (c), and (e), 250 pm for (d), and 340 pm for (f). Sample bias was -200 mV for (a) to (d), 100mV for (e), and 200 mV for (f).

resolution images reveal the pentacene molecules as a series of alternating bright and dim bands, with one long edge of the molecule showing slightly higher contrast in the AFM signal [Figs. 1(b) to (d)]. A closer look to the molecular structures reveals that instead of assembling in a compact cluster, pentacene molecules aggregate into one-dimensional stacks on the terraces. Their long axes are parallel to the [010] crystallographic direction and along the rows of surface-topping two-fold coordinated oxygen (O_{2c}) atoms.[20] Details of different stack structures indicate that molecules preferentially join with a small offset perpendicular to the stack direction. The surface features visible in the background of the AFM images help to place the molecular registry between two adjacent rows of O_{2c}, above the characteristic sloped groove structure of this anatase surface. The higher AFM contrast at the upper long edge of the molecule suggests a slight tilt in its adsorption geometry.

At ultra-low coverages, isolated pentacene molecules randomly populate the terraces of the anatase substrate, exhibiting the same orientation observed for the molecules composing the stacks. Typical examples of sub-molecular resolution AFM images of isolated pentacene molecules are displayed in Figs. 1(e) and (f). Depending on the probe termination, they present a series of features (rings or stripes) along the molecule's long axis. Isolated pentacene molecules are also found decorating the atomic steps of the surface. The island shown in Fig. 1(a) displays the three geometrically inequivalent steps of the anatase (101) facet.[21] At the upper and side steps of the island, the pentacene molecules adsorb following a side-on configuration with their long axis aligned with the step direction; these molecules are highlighted in Fig. 1(b) by blue arrows. Interestingly, sub-molecular resolution AFM images of pentacene molecules found at the energetically most stable step[21] reveal a configuration that is rotated approximately 45° from the orientation of the stacks, with the molecules adsorbing across the step simultaneously connecting upper and lower terraces, as pointed out by arrows in Figs. 1(a) and (c).

We employed dispersion-corrected DFT simulations to understand the molecule-oxide interactions and binding strength. Following the adsorption configuration detected for pentacene molecules by the experiments, the molecule was initially placed between the O_{2c} rows and over the sloping groove of the (101) anatase surface, with the short axis slightly tilted to bring the molecular plane parallel to the facet. Fig. 2(a) and Fig. 2(b) illustrate two possible molecular registries in the [010] crystallographic direction: configuration A, where the center of the pentacene molecule is placed above a five-fold coordinated surface titanium atom (Ti_{5c}); and configuration B, where the center of the molecule is displaced mid-way between two Ti_{5c} atoms. Structural optimization results, summarized in Table 1, revealed that pentacene physisorbs in both registries with a similar structure and with adsorption energies E^{A}_{ADS}=-1.57eV and E^{B}_{ADS}=-1.91eV. Dispersion interactions, known to be important for molecular adsorbates on this surface,[22] contribute 98% and 87% to the adsorption energy respectively. While configuration A is stabilized entirely by van der Waals forces, configuration B is further stabilized by weak chemical bonds with four Ti_{5c} atoms. In the energetically preferred configuration B, the molecule adsorbs in a flat conformation parallel to the sloping groove, with the extremes slightly lowered towards the surface by 10pm. The molecular axis lies 0.26nm above the surface-topping plane of O_{2c} atoms and directly above four undercoordinated Ti_{5c} atoms, as illustrated in Figs. 2(b) and (c). The tilt angle of 22.6° is similar to the sloped groove, and explains the higher contrast in the AFM signal detected over the upper long edge of the molecules. Since the difference between computed adsorption energies is large compared to the temperatures of the sample preparation, we conclude that isolated pentacene molecules at the terraces preferentially attach in registry B.

To gain insight into the formation of pentacene monolayers on the anatase surface, we carried out an investigation of the one-dimensional pentacene stack geometries. A single pentacene molecule was placed onto each of the two sloped surface grooves in the unit cell to simulate full monolayer coverage. Since the atomic arrangement of one groove is shifted in the [010]

Table 1: Comparison of adsorption structures and energies for single pentacene in configurations A and B. Here d and Θ are the molecule adsorption height and tilt angle, as illustrated in Fig. 2(c). We computed the total adsorption energy E_{ADS} and its dispersion contribution E_{ADS}^{VDW} (fractional proportion shown in italic brackets).

Config.	d [nm]	Θ [°]	E_{ADS} [eV]	E_{ADS}^{VDW} [eV] *(%)*
A	0.24	23.7	-1.57	-1.54 *(98)*
B	0.26	22.6	-1.91	-1.67 *(87)*

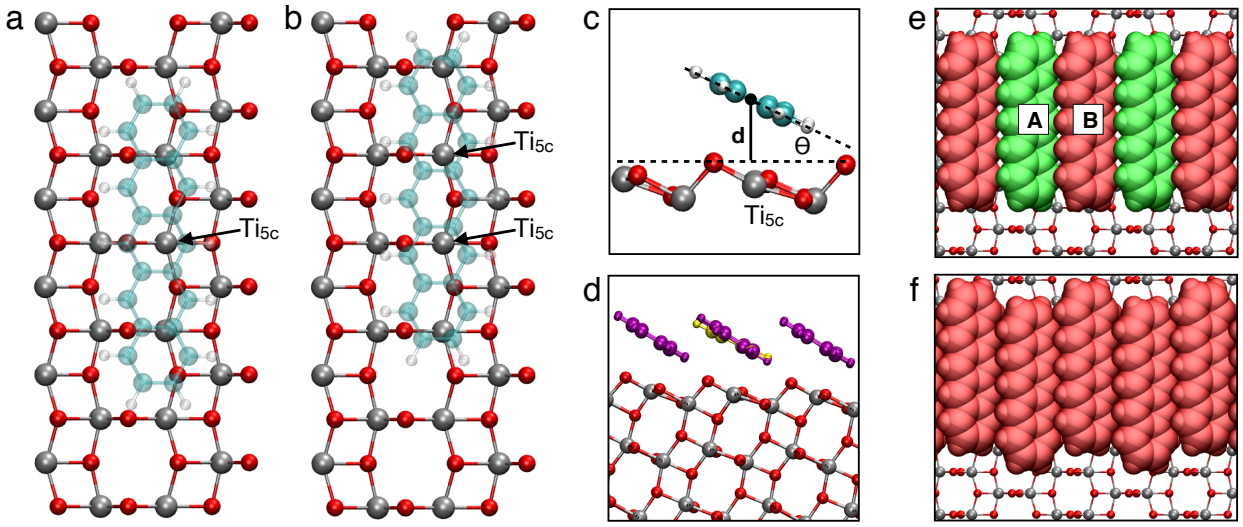

Figure 2: (a) Pentacene adsorption registry A, with the center above a Ti_{5c} atom. (b) Pentacene adsorption registry B, with the center of the molecule above the mid-point between Ti_{5c} atoms. (c) Side view of a physisorbed pentacene molecule, indicating adsorption height *d* and angle Θ. (d) Side view comparison between the geometries of adsorbed pentacene stack (purple) and isolated molecule (yellow). (e) Pentacene mixed registry A-B stacking (straight stack). (f) Pentacene single registry B-B stacking (offset stack).

direction by half unit cell with respect to the adjacent one, a Ti_{5c} surface site on one groove is aligned with a mid-point between Ti_{5c} atoms on the other. Consequently, molecules adsorbed in a straight line stack correspond to a mixed A-B registry, as illustrated in Fig. 2(e). A stack of molecules in the same registry can only be obtained if the adjacent pentacenes adsorb with an offset of a half-unit cell, like in Fig. 2(f). We optimized candidate stack structures of mixed A-B and single B-B registries, formed by assuming a maximum overlap of molecules in the stack. Computed adsorption energies per molecule of E_{ADS}^{AB}=-1.96eV and E_{ADS}^{BB}=-2.19eV confirm that molecular stacking with an offset is energetically favorable on this surface. This finding supports the experimental observation of diagonal stack growth, and the presence of kinks in the stacks, in numerous AFM images (Fig. 1).

Stronger binding energies for stacked pentacene molecules compared to isolated ones arise partly from the inter-molecular attraction within the stack. To quantify the strength of this interaction, we computed the reference energy for the molecular stack without the substrate and compared it to energy of gas phase pentacene molecules. This also facilitated the decomposition of the adsorption energy E_{ADS}^{BB}=-2.19eV into intra-stack and stack-surface contributions. We established that molecule-molecule interactions contribute 16% (-0.36eV) and the molecule-surface interactions account for 84% (-1.83eV) of the adsorption energy per molecule in a stack configuration. While the presence of other molecules in the stack appears to reduce the strength of pentacene binding to TiO_2 from -1.91eV to -1.83eV per molecule, the monolayers are overwhelmingly stabilized by molecule-surface interactions (in line with recent experimental observations for conjugated adsorbates on (101) anatase[23]). Consequently, each molecule in a stack adopts a local geometry that is almost identical to the isolated molecule, with minimal changes in the tilt angle (see Fig. 2(d)).

The alignment of electronic levels at the molecule-oxide interface is critical to effective flow of charge between the materials. The decomposed electronic states of the surface and the

molecule adsorbed at a B registry are shown in Fig. 3(d). The highest occupied electronic states of the molecule HOMO, HOMO-1 and HOMO-2 appear as narrow peaks in the band gap of the oxide. Frontier molecular states of the physisorbed pentacene remain as discrete and sharp as those of the gas phase molecule (within the molecular level broadening 0.05eV), apart from LUMO which exhibits a double peak. This indicates that the TiO_2 anatase substrate does not significantly hybridize frontier molecular orbital states of pentacene in this adsorption configuration, in contrast to chemisorption on metallic substrates where significant orbital broadening and charge transfer were observed.[24–26] Bader charge analysis[27,28] revealed that pentacene transfers only 0.1 e^- to the TiO_2 substrate.

The Fermi level at the interface is located at the highest occupied molecular orbital (HOMO) 0.7eV below the TiO_2 conduction band. We analyzed the spatial distribution of this state, illustrated in Fig. 3(e), to find that it is mostly localized on the molecule and shaped much like the gas phase pentacene HOMO. While the molecule-surface charge transfer is nearly zero, the HOMO indicates that a small amount of charge is localized in weak molecule-substrate bonds. Four regions of electronic density extend from the molecular backbone towards four Ti_{5c} atomic sites directly below the pentacene. The d_{z2} character of these features points to covalent interactions between the delocalized electrons of the pentacene backbone and the d states of Ti_{5c} atoms. This finding clarifies the small covalent contribution to the binding energy of adsorption configuration B. Considerable dispersion forces dominate pentacene-TiO_2 interactions (87%), stabilizing the molecule in a physisorbed configuration far enough from the surface so that the organic and inorganic layers remain electronically decoupled; nevertheless, such a distance allows the formation of weak covalent bonds (13% of adsorption energy) that supply a direct pathway for electron transfer between the two layers. The lowest unoccupied molecular orbital (LUMO) is placed 0.3eV above the bottom of the conduction band of the oxide, facilitating the transfer of electron charge carriers from the photoactive organic layer into the anatase buffer zone. The LUMO shape (Fig. 3(f)) reveals two principal

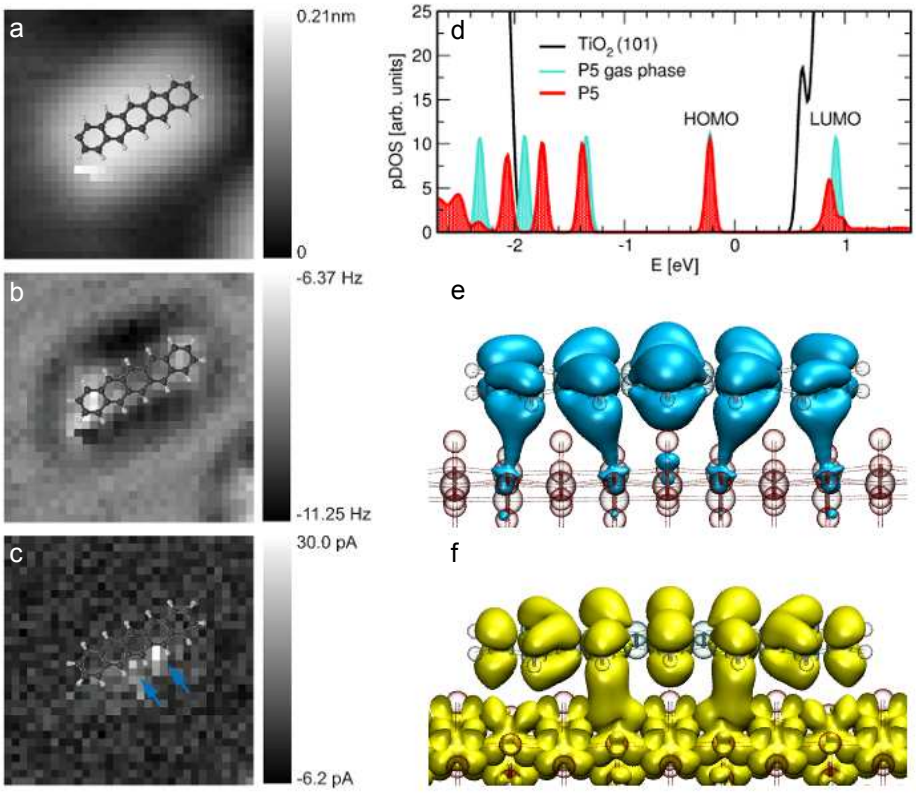

Figure 3: (a) Topography of an isolated pentacene molecule on the surface, over which a bias spectroscopy imaging measurement based on the acquisition of a Δf(V) curve over each pixel of the image was obtained (image size 3 $\times$ 3 nm^2). (b) Δf signal corresponding to a slide of all the measured Δf(V) curves at a sample bias of V=500mV. (c) $<I_t>$ signal associated with the image shown in (b). For additional experimental details see Fig. S1. (d) Partial DOS contributions of the TiO_2 (101) surface and adsorbed pentacene (P5), compared with DOS of pentacene in the gas phase. Gas phase DOS was aligned with the total system DOS at the Fermi level. (e) System HOMO spatial distribution (10^{-4} e-/Å^3 isosurface), obtained by integrating total DOS in the energy interval [0, -600] meV. (f) System LUMO spatial distribution, (10^{-4} e-/Å^3 isosurface), obtained by integrating total DOS in the energy interval [650, 1000] meV (note that image illustrates both the molecular LUMO and substrate conduction band states).

channels for charge injection below the central part of the molecule. Evidence of localized charge injection can be spotted in the experimental STM image displayed in Figs. 3(a - c), taken combining multi-pass imaging[17] with bias spectroscopy imaging,[29] see Fig. S1. for details. The favorable alignment of molecular levels with respect to the substrate and the corresponding charge injection pathways are strong indicators of efficient charge transfer across the pentacene/TiO_2 interface.

Force spectroscopy data acquired on a volume over the surface provides insight into the AFM imaging contrast mechanisms. The positions that would correspond to the hollow sites at the central part of the molecule exhibit a canonical probe-surface interaction force, with a well-defined single force minimum along the probe-sample separation distance explored (Figs. 4(a), 4(b), and Fig. S2 of the supporting information). Upon probing the forces at hollow sites close to the sides of the molecule, the onset of a second force minimum starts to develop (Fig. S2). The appearance of a double force minima is clear when probing the sites that would correspond to the CH groups at the upper long edge of the molecules (Fig. 4(a) and Fig. S2). The development of a second minimum in the probe-surface interaction force over both the hollow and the CH site may correspond to a slight bending of the molecule as the probe exerts force on it, or to the atomic-scale bending of the probe termination. Multiple minima in the interaction force are usually associated with transitions between different solution of the probe-surface potential energy upon reducing the probe-sample separation.[30] The absence of energy dissipation[31] (Fig. S3) during the acquisition of the force volume points towards an elastic bending due to the interaction with the probe.

Force spectroscopy experiments were simulated by approaching a probe model to key pentacene sites —an uppermost C atom site and the central ring of the molecule, Fig. 4(c)— to clarify in detail probe-molecule interactions and associated atomic rearrangements in the presence of the substrate. We deployed first a TiO_2 cluster probe model with a chemically-

passive OH group termination; such a probe was shown to produce the dominant AFM contrast in atomic resolution imaging of the bare (101) anatase surface.[20] Computed AFM force spectroscopy curves presented in Fig. 4(c) testify to a stronger attractive interaction above pentacene rings as opposed to the carbon backbone, in agreement with the experimental force curves, displayed in Fig. 4(a). The maximum attraction over the ring site is reached by lowering the probe by a further 50pm, reflecting the topographic 50pm height difference between the carbon and the ring site in the atomistic model. Upon inspection of the calculated forces, the pentacene AFM contrast seems to be in line with the standard AFM imaging modes of pentacene and carbon nanostructures composed of aromatic rings[16,32,33] recorded with different probe terminations, where additional repulsive force contributions above C atom sites locally reduce interaction strength. AFM simulations were repeated over the same sites in a pentacene B-B stack to explore how probe-surface interactions change with monolayer formation. Theoretical force spectroscopy curves for isolated and stacked pentacene are compared in Fig. 4(c). In the stack, the onset of attraction is shifted to lower probe heights but the repulsive interactions are slightly reduced, indicating that the intermolecular bonding within the stack weakens the pentacene-probe interactions.

Simulated AFM spectroscopy curves over the pentacene stack can be directly compared to the short-range interaction data extracted from a force volume, and depicted in Fig. 4(b). Although the general behavior of the curves is fairly reproduced, we found the computed maximum attractive interactions of 0.20-0.25nN considerably larger than the 0.06-0.10nN short-range force values recorded in the experiments. Such a result points to a different chemical termination of the AFM probe than the initial model considered for these computations. This presents a conundrum, since AFM probes were in situ conditioned to be coated by TiO_2 from the substrate, and no other apex termination has been identified to produce weaker probe-surface interactions than the OH group.[20] In the absence of other contaminant material that might alter the chemical composition at the probe apex, we hypothesized that

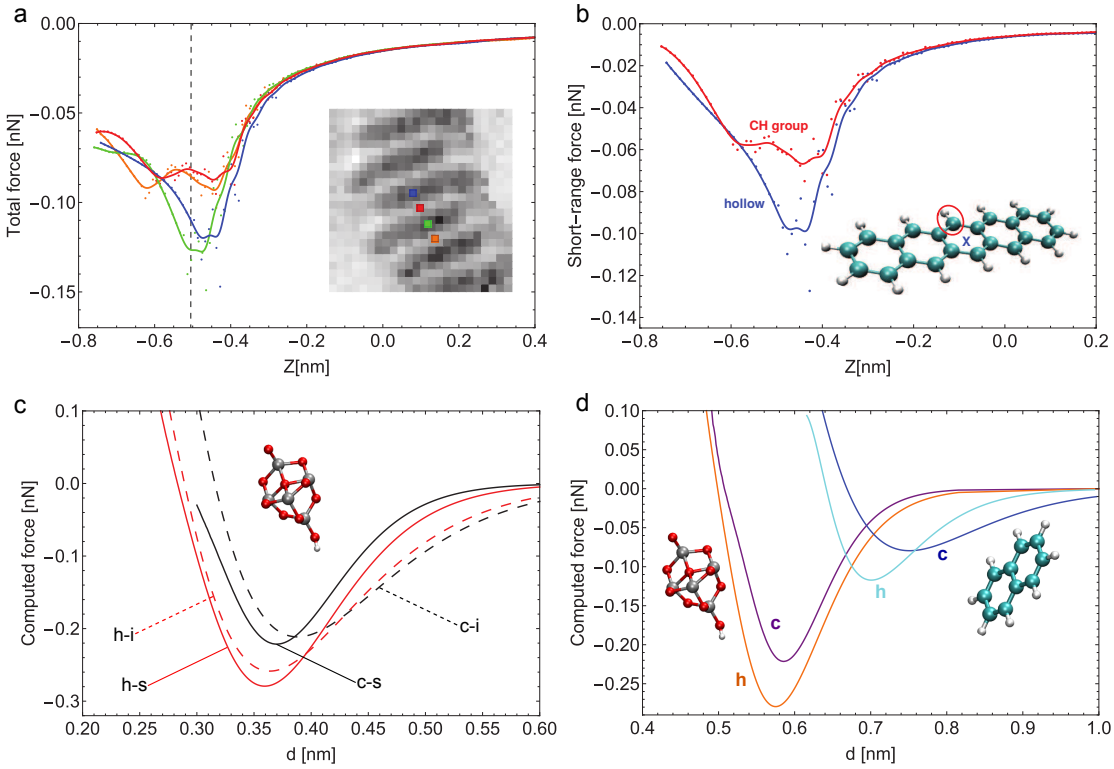

Figure 4: (a) Force curves extracted from a force volume composed by (24×24) Δf(Z) curves measured over an area of (3x3) nm^2 on a stack of pentacene molecules deposited on the TiO_2 (101) anatase surface. Acquisition parameters are: f_o = 152471 Hz, A = 95.9 Å, K = 23.7 N/m, Q = 44163. Sample bias was -200 mV. The inset image is a slide of the total force values at the probe-sample separation indicated by the doted vertical line in (a). (b) Details of the short-range forces of two curves shown in (a) obtained close to a CH group site and a hollow site. The dots denote the force points after conversion from the Δf(Z) curves, and the lines correspond to a spline interpolation of the experimental points. (c) Simulated force curves over a carbon atom and a hollow site —see positions in the model depicted in (b)— of an individual molecule (c-i, h-i; dashed lines) and a molecule within a B-B stack configuration (h-s, c-s), respectively. These forces were calculated using the OH group terminated TiO_2 cluster depicted in (c) as probe model. (d) Comparison of the forces simulated using the TiO_2 cluster and a naphthalene molecule as probe model. A molecular probe produces short-range forces of a magnitude comparable to the experimental counterparts.

the probe may have picked up a molecule during the scan.[34] To verify the possibility of AFM imaging by a probe terminated in pentacene, force spectroscopy simulations over an isolated molecule were repeated with a naphthalene molecule as model probe. Such a probe allowed us to include contrast-defining interactions between the low-lying aromatic rings of the pentacene molecule, while presenting the weakly-interacting C-H bond towards the substrate in an analogy to the OH group terminated probes that produce atomic resolution AFM images in the anatase surface.[20] Computed spectroscopy curves with a naphthalene probe are compared to those resulting from the OH-terminated TiO_2 cluster model in Fig. 4(d). The ordering and relative position of the curve minima between the two key sites remains the same, pointing to the same AFM contrast mode in the imaging of pentacene for both probe models. Notwithstanding, the naphthalene-terminated probe exhibits maximum attractive interactions of 0.07-0.11nN that are 2-3 times smaller than for the TiO_2 cluster case; values that show a reasonable agreement with the experimental results. Small discrepancies, as well as the lack of elastic effects associated with double minimum force spectroscopy signatures, can be explained by the randomly chosen orientation of the molecular probe model and the approximation of a pentacene probe with a naphthalene molecule.

To gain insight into pentacene thin-film formation on the anatase (101) surface, we conducted an experimental AFM characterization of the pentacene growth beyond the first molecular layer, and found that the second pentacene layer presents a completely different morphology. Fig. 5(a) displays a surface region where these two layers coexist. A distinct boundary —an abrupt step approximately 1.45 nm high (Fig. 5(b)) crossing the image from the upper-left to the lower-right side— separates these two well-differentiated regions. AFM images reveal that the domain with lower topographic contrast corresponds to a phase of pentacene adsorbed into planar molecular stacks that covers the anatase surface almost in full, as depicted in Fig. 5(c). Similar AFM images taken on the region showing higher topographic contrast present well ordered periodic features showing a rectangular-like pattern, with a

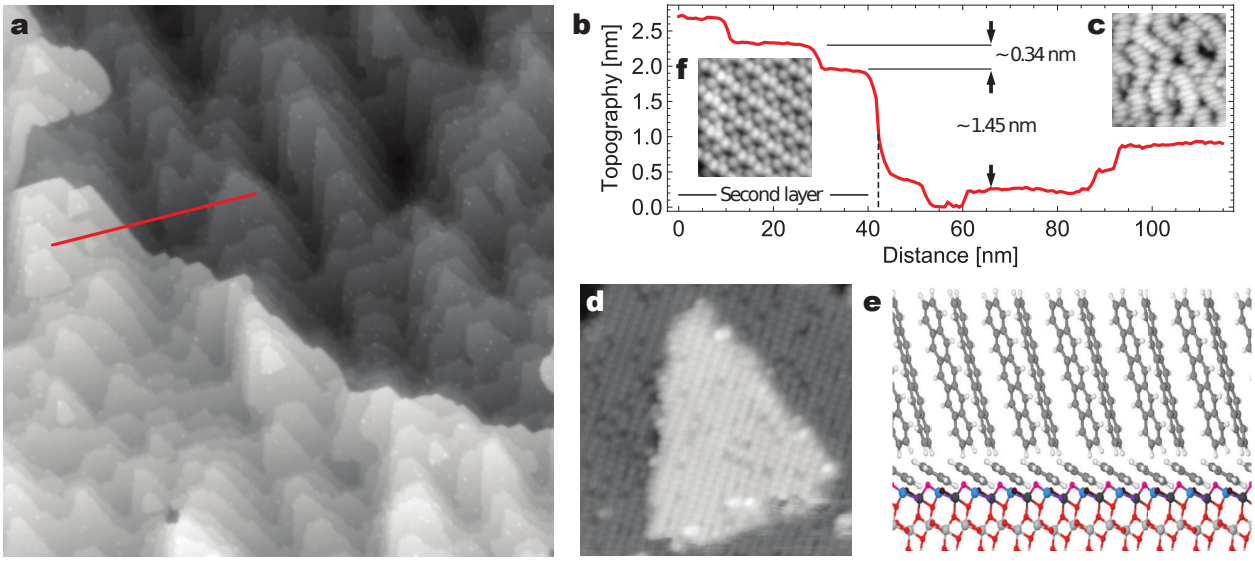

Figure 5: (a) Topographic AFM image showing a boundary between the first and second layers of pentacene molecules adsorbed on the (101) TiO_2 anatase surface. Image size is (300nm×300nm). (b) Line profile marked in (a). (c) Topographic AFM image revealing the structure of the first layer of pentacene molecules, that corresponds to the lower topographic contrast in (a). Image size is (10nm×10nm). (d) Topographic (static) STM image showing the typical surface morphology of the second layer of pentacene molecules. Image size is (25nm×25nm). (e) Artistic representation denoting a possible vertical, slightly tilted configuration of the second layer of pentacene molecules grown over an almost fully pentacene passivated (101) TiO_2 anatase surface. (f) Image of the variation of the frequency shift over a (4nm×4nm) area of the second layer of pentacene molecules upon applying a multi-pass method, bringing the probe 230 pm closer to the surface during the second pass with respect to the topographic set point. The contrast of this image was been inverted to mimic the appearance of a topographic image. Acquisition parameters are: f_o = 152828 Hz, k = 23.8 N/m, Q = 34833. Δf set point was -6.5 Hz (a), -2.0 Hz (c), -8.0 Hz (f). Oscillation amplitude was 112.5 Å (a), 168.8 Å (c), and 67.6 Å (f). Sample bias was -0.3 V (a) and (c), -0.2 V (f), 2.5 V (d). Current set point was 20 pA for (d).

the repeating unit much smaller than the pentacene molecule length, e.g., as illustrated in Fig. 5(d). The 1.45 nm height difference between the domains does not relate to the morphology of the anatase surface (with an atomic step height of approximately 0.34 nm), but rather points towards the second layer of pentacene molecules growing in a slightly tilted, vertically-oriented configuration over a pentacene-passivated anatase surface, e.g. as illustrated in Fig. 5(e). While the reactive anatase (101) surface promotes horizontal monolayer growth, it is sufficiently passivated by the first molecular layer so that further layers grow vertically. High resolution molecular AFM images acquired with the multi-pass method[17] over the region with higher topographic contrast reveal an internal and complex structure within the rectangular unit cell (Fig. 5(f)), denoting a high-density packing of the vertically oriented pentacene molecules. Although the packing, orientation and tilting of the molecules in the second layer is difficult to discern from our AFM images, our results suggests that subsequent pentacene monolayers may resemble the bulk configuration of pentacene organic solids.

With prospective applications of pentacene as thin-film component in organic transistors[35] and light-emitting diodes[36] among other organic devices, we extend our discussion to AFM studies addressing pentacene thin-film growth on different buffer materials.[37] Unlike metals, metal oxides present relatively inert substrates for pentacene attachment. Studies on SiO,[38] ITO,[39] $LaSrMnO_3$,[40] Al_2O_3[41] and HfO_2[42] surfaces all found that molecules adsorb in standing or tilted configurations, at odds with our findings. Dendritic aggregation and monolayer growth has been well characterised on SiO[43] and Al_2O_3, in contrast to the planar stacking growth mechanism observed for the first layer of pentacene on TiO_2 (101) anatase. On this substrate, not only do we observe horizontal monolayer growth, but the molecules aggregate parallel to each other in the departure from the herringbone arrangement in bulk[44] and vertical monolayers. These features can be attributed to the strong molecule-substrate dispersion interactions and the topological constraint of the sloping grooves of the surface.

A recent study supports our finding that pentacene adsorbs horizontally on the sloping terrace of anatase[11] (albeit with a greater adsorption energy of -2.48eV, the structural details were not disclosed). Similar adsorption behavior was reported for pentacene on the (110) surface of the rutile polymorph.[45] We conclude that TiO_2 presents a more reactive substrate for dispersion-dominated pentacene thin films than other metal oxides, which is consistent with the benzene adsorption trend on metal oxide substrates.[11] The stronger bonds and orbital overlap with TiO_2 should enhance charge injection across the hybrid organic/inorganic interface.

Conclusion

The atomistic details of the hybrid organic/inorganic boundary inside heterostructure devices critically define the electronic properties of this interface, and through it, those of the entire device. We have employed several AFM and STM experimental techniques in combination with first-principles simulations to characterize the interface between pentacene thin films and TiO_2 anatase; two materials with superior electrical properties frequently used in optoelectronic devices. A multipass AFM imaging technique allowed us to overcome the technical challenge of simultaneously imaging the substrate, steps, molecular adsorbates and layers with atomic scale resolution. An inert AFM probe termination, here an adsorbed pentacene molecule, met the other necessary condition for submolecular imaging. Consequently we were able to detect the relative orientation of molecular adsorbates with respect to each other and the substrate, which greatly facilitated the computational study of adsorption.

Sub-molecular resolution AFM images reveal that the first layer of pentacene molecules physisorb horizontally on the anatase surface, with the conjugated backbone of the molecule parallel to the typical sloping terraces of anatase. Individual pentacene molecules are also found decorating the step-edges of the anatase (101) surface, with an adsorption geometry

that varies with the particular step structure. At the surface terraces, pentacene molecules self-organize into planar molecular stacks for coverages below one monolayer. The anatase surface is passivated by these molecular stacks that compose the first pentacene layer, so that the second pentacene layer adopts a high-density packing of vertically oriented molecules, promoting a thin film growth that is compatible with the bulk structure of the pentacene organic crystal.

Among the metal oxides typically used as buffer layers in electronic heterostructure devices, TiO_2 stands out as the only substrate known to date that binds pentacene in a horizontal geometry at the organic/inorganic interface. Substantial molecule-surface dispersion interactions stabilize the physisorbed adsorption configuration further above the surface, where electronic structure coupling between the pentacene and anatase is limited. Adsorbed pentacene introduced sharp molecular states into the band gap of the substrate, but it is the molecular LUMO that supplied the direct orbital overlap with the substrate necessary for charge transfer. The position of the pentacene LUMO in the conduction band of anatase implies barrier-free injection of electron charge carriers from the organic molecules into the substrate. Higher levels of theory are needed to accurately compute the alignment of electronic levels between the pentacene thin films and the TiO_2 substrate. Nevertheless, the localized charge injection pathways and the favorable level alignment at this interface are indicators that these materials would contribute efficient thin film devices for photovoltaic applications.

Methods

A UNISOKU Ltd. ultrahigh vacuum (UHV) cryogenic dynamic AFM equipped with a home-built optical interferometer for the detection of the cantilever dynamics was used for the experiments. Measurements were accomplished at a 77 K probe-sample tempera-

ture using the frequency modulation detection scheme.[46] Platinum iridium coated silicon cantilevers (PPP-NCLPt-20, Nanosensors, Switzerland) were excited to their instantaneous first mechanical resonant frequency keeping the oscillation amplitude (A) constant. The tunnelling current flowing between probe and surface averaged over multiple cantilever oscillation cycles[47] ($<I_t>$) was simultaneously detected during topographic AFM imaging using a commercial scanning probe microscopy controller (Nanonis SPM Control System, SPECS, Germany). The shift of the first mechanical resonant frequency (Δf) from the free-oscillation value upon forces acting on the cantilever probe was used to regulate the probe-surface separation. Sub-molecular resolution AFM imaging was performed using a multi-pass method.[17] Force spectroscopy[48,49] was performed by recording Δf as a function of the probe-sample relative vertical displacement (Z) over a rectangular matrix of pixels superimposed to a previously imaged area of the surface, closing the feedback loop upon displacement of the probe between adjacent pixels.[17] The total probe-surface interaction force was obtained by applying an inversion procedure[50] to the recorded $\Delta f(Z)$ curves. Topographic effects due to the acquisition procedure were properly compensated.[17,51] Further details about protocols for in situ probe conditioning and anatase sample preparation can be found elsewhere.[20] Molecular deposition was carried out by exposing a clean anatase surface to pentacene molecules sublimated from a homebuilt evaporation cell upon reaching 160°C in UHV. The substrate was kept at room temperate during the pentacene deposition, and coverage was regulated by adjusting the exposure time.

All DFT simulations were carried out with the VASP code,[52] the PBE exchange-correlation functional[53] and semi-empirical DFT-D2 dispersion corrections.[54] We employed PBE PAW potentials and a planewave cutoff of 500eV. An onsite U=4eV was applied to the substrate Ti atoms to adjust the position of gap states with respect to the conduction band minimum of TiO_2, following other studies of anatase surfaces.[55,56]

We employed the TiO_2 anatase (101) surface model previously used for adsorption studies on this surface.[20] The 10.57Å × 23.12Å × 40Å model surface area accommodates two sloped surface grooves for pentacene attachment. Single pentacene images were laterally separated by dx=6Å and dy=9Å between different simulation cells, while adjacent pentacene stack images were separated by dy=7.4Å. The tall unit cell allowed 24Å between surface slabs in adsorption simulations, and 13.8Å between them in AFM simulations. The same unit cells was used for isolated pentacene and surface reference calculations. Geometry optimizations were performed with a gamma-point k-point grid until atomic forces were reduced below 0.01eV/Å . Such k-space sampling was selected by downscaling the converged (6×6×2) k-point setting for bulk unit cell calculations of TiO_2 anatase when upscaling the unit cell towards the large (1x6) unit area surface geometry. Adsorption energies and electronic properties were obtained using a 4×2×1 k-point mesh.

Acknowledgement

Work supported by the NIMS (PF201 and PF303 projects), by the JST PRESTO Grant Number JPMJPR1418, JSPS KAKENHI Grant Number 16K05674, and by the Spanish MINECO (projects CSD2010-00024 and MAT2014-54484-P). C.M was supported by the Japanese Ministry for Education, Science and Technology through International Center for Young Scientist (ICYS) program and by the Agency for Management of University and Research grants (AGAUR) of the Catalan government through the FP7 framework program of the European Commission under Marie Curie COFUND action 600385. Computer time was provided by the Spanish Supercomputing Network (RES, Spain) at the MareNostrum III (BCS, Barcelona) and Magerit (CesViMa, Madrid) Supercomputers. O.S thanks the Charles University-NIMS International Cooperative Graduate School Program.

Supporting Information Available

Fig. S1, AFM images obtained from the combination of a multipass technique with bias-spectroscopy imaging; Fig. S2, comparison of force curves over different equivalent surface locations obtained from a force volume spectroscopy measurement; Fig. S3, force curves, force images, amplitude and dissipation signal associated with the force volume.

References

(1) Brédas, J.-L.; Norton, J. E.; Cornil, J.; Coropceanu, V. Molecular Understanding of Organic Solar Cells: The Challenges. *Acc. Chem. Res.* **2009**, *42*, 1691–1699.

(2) O'Regan, B.; Grätzel, M. A Low-Cost, High-Efficiency Solar Cell Based on Dye-Sensitized Colloidal TiO_2 Films. *Nature* **1991**, *353*, 24.

(3) Crossland, E.; Noel, N.; Sivaram, V.; Leijtens, T.; Alexander-Webber, J.; Snaith, H. J. Mesoporous TiO_2 Single Crystals Delivering Enhanced Mobility and Optoelectronic Device Performance. *Nature* **2013**, *495*, 215–219.

(4) Yoo, S.; Domercq, B.; Kippelen, B. Efficient Thin-Film Organic Solar Cells Based on Pentacene/C_{60} Heterojunctions. *Appl. Phys. Lett.* **2004**, *85*, 5427.

(5) Cheyns, D.; Gommans, H.; Odijk, M.; Poortmans, J.; Heremans, P. Stacked Organic Solar Cells Based on Pentacene and C_{60}. *Sol. Energ. Mat. and Sol. Cells* **2007**, *91*, 399–404.

(6) Mishra, A.; Fischer, M. K. R.; Bäuerle, P. Metal-Free Organic Dyes for Dye-Sensitized Solar Cells: From Structure: Property Relationships to Design Rules. *Angew. Chem. Int. Ed.* **2009**, *48*, 2474–2499.

(7) Freitag, M.; Boschloo, G. The Revival of Dye-Sensitized Solar Cells. *Curr. Opinion Electrochem.* **2018**, *2*, 111–119.

(8) Estrella, L. L.; Balanay, M. P.; Kim, D. H. Theoretical Insights into D-D-π-A Sensitizers Employing N-Annulated Perylene for Dye-Sensitized Solar Cells. *J. Phys. Chem. A* **2018**, *122*, 6328–6342.

(9) Lee, C.-P.; Li, C.-T.; Ho, K.-C. Use of Organic Materials in Dye-Sensitized Solar Cells. *Mater. Today* **2017**, *20*, 267–283.

(10) Zhang, K.; Zhang, W.; Huang, J.; Pang, A.; Wong, M. S. Metal-Free Photosensitizers Based on Benzodithienothiophene as π-conjugated Spacer for Dye-Sensitized Solar Cells. *Org. Electron.* **2017**, *42*, 275–283.

(11) Domenico, J.; Foster, M. E.; Spoerke, E. D.; Allendorf, M. D.; Sohlberg, K. Effect of Solvent and Substrate on the Surface Binding Mode of Carboxylate-Functionalized Aromatic Molecules. *J. Phys. Chem. C* **2018**, *122*, 10846–10856.

(12) Kunzmann, A.; Gruber, M.; Casillas, R.; Tykwinski, R. R.; Costa, R. D.; Guldi, D. M. Tuning Pentacene Based Dye-Sensitized Solar Cells. *Nanoscale* **2018**, *10*, 8515–8525.

(13) Binnig, G.; Quate, C. F.; Gerber, C. Atomic Force Microscope. *Phys. Rev. Lett.* **1986**, *56*, 930–933.

(14) Pavliček, N.; Gross, L. Generation, Manipulation and Characterization of Molecules by Atomic Force Microscopy. *Nat. Rev. Chem.* **2017**, *1*, 0005.

(15) Gross, L.; Mohn, F.; Moll, N.; Liljeroth, P.; Meyer, G. The Chemical Structure of a Molecule Resolved by Atomic Force Microscopy. *Science* **2009**, *325*, 1110.

(16) Moll, N.; Gross, L.; Mohn, F.; Curioni, A.; Meyer, G. The Mechanisms Underlying the Enhanced Resolution of Atomic Force Microscopy with Functionalized Tips. *New J. Phys.* **2010**, *12*, 125020.

(17) Moreno, C.; Stetsovych, O.; Shimizu, T. K.; Custance, Ó. Imaging Three-Dimensional Surface Objects with Submolecular Resolution by Atomic Force Microscopy. *Nano Lett.* **2015**, *15*, 2257–2262.

(18) Sadewasser, S., Glatzel, T., Eds. *Kelvin Probe Force Microscopy*; Springer Series in Surface Sciences; Springer Berlin Heidelberg, 2012; Vol. 48.

(19) Binnig, G.; Rohrer, H.; Gerber, C.; Weibel, E. Surface Studies by Scanning Tunneling Microscopy. *Phys. Rev. Lett.* **1982**, *49*, 57–61.

(20) Stetsovych, O.; Todorović, M.; Shimizu, T. K.; Moreno, C.; Ryan, J. W.; León, C. P.; Sagisaka, K.; Palomares, E.; Matolín, V.; Fujita, D.; Pérez, R.; Custance, Ó. Atomic Species Identification at the (101) Anatase Surface by Simultaneous Scanning Tunnelling and Atomic Force Microscopy. *Nat. Commun.* **2015**, *6*, 7265.

(21) Gong, X.-Q.; Selloni, A.; Batzill, M.; Diebold, U. Steps on Anatase TiO_2 (101). *Nat. Mater.* **2006**, *5*, 665–670.

(22) Hemeryck, A.; Motta, A.; Lacaze-Dufaure, C.; Costa, D.; Marcus, P. DFT-D Study of Adsorption of Diaminoethane and Propylamine Molecules on Anatase (101) TiO_2 Surface. *Appl. Surf. Sci.* **2017**, *426*, 107–115.

(23) Zajac, L.; Bodek, L.; Such, B. Adsorption Behavior of Zn Porphyrins on a (101) Face of Anatase TiO_2. *Appl. Surf. Sci.* **2018**, *443*, 452–457.

(24) Müller, K.; Seitsonen, A. P.; Brugger, T.; Westover, J.; Greber, T.; Jung, T.; Kara, A. Electronic Structure of an Organic/Metal Interface: Pentacene/Cu(110). *J. Phys. Chem. C* **2012**, *116*, 23465–23471.

(25) Song, Y. J.; Lee, K.; Kim, S. H.; Choi, B.-Y.; Yu, J.; Kuk, Y. Mapping Atomic Contact Between Pentacene and a Au Surface Using Scanning Tunneling Spectroscopy. *Nano Lett.* **2010**, *10*, 996–999.

(26) Sun, X.; Suzuki, T.; Yamauchi, Y.; Kurahashi, M.; Wang, Z. P.; Entani, S. Ab Initio Study of Pentacene on the Fe(100) Surface. *Surf. Sci.* **2008**, *602*, 1191–1198.

(27) Tang, W.; Sanville, E.; Henkelman, G. A Grid-Based Bader Analysis Algorithm Without Lattice Bias. *J. Phys.: Condens. Matter* **2009**, *21*, 084204.

(28) Bader, R. F. W. *Atoms in Molecules: A Quantum Theory*; Oxford University Press, New York: New York, 1990.

(29) Sadewasser, S.; Jelínek, P.; Fang, C.-K.; Custance, Ó.; Yamada, Y.; Sugimoto, Y.; Abe, M.; Morita, S. New Insights on Atomic-Resolution Frequency-Modulation Kelvin-Probe Force-Microscopy Imaging of Semiconductors. *Phys. Rev. Lett.* **2009**, *103*, 266103.

(30) Sugimoto, Y.; Pou, P.; Custance, Ó.; Jelínek, P.; Abe, M.; Pérez, R.; Morita, S. Complex Patterning by Vertical Interchange Atom Manipulation Using Atomic Force Microscopy. *Science* **2008**, *322*, 413–417.

(31) Oyabu, N.; Pou, P.; Sugimoto, Y.; Jelínek, P.; Abe, M.; Morita, S.; Pérez, R.; Custance, Ó. Single Atomic Contact Adhesion and Dissipation in Dynamic Force Microscopy. *Phys. Rev. Lett.* **2006**, *96*, 106101.

(32) Albers, B. J.; Schwendemann, T. C.; Baykara, M. Z.; Pilet, N.; Liebmann, M.; Altman, E. I.; Schwarz, U. D. Three-Dimensional Imaging of Short-Range Chemical Forces with Picometre Resolution. *Nat. Nanotechnol.* **2009**, *4*, 307–310.

(33) Ondráček, M.; Pou, P.; Rozsíval, V.; González, C.; Jelínek, P.; Pérez, R. Forces and Currents in Carbon Nanostructures: Are We Imaging Atoms? *Phys. Rev. Lett.* **2011**, *106*, 176101.

(34) Pawlak, R.; Ouyang, W.; Filippov, A. E.; Kalikhman-Razvozov, L.; Kawai, S.; Glatzel, T.; Gnecco, E.; Baratoff, A.; Zheng, Q.; Hod, O.; Urbakh, M.; Meyer, E.

Single-Molecule Tribology: Force Microscopy Manipulation of a Porphyrin Derivative on a Copper Surface. *ACS Nano* **2016**, *10*, 713–722.

(35) Klauk, H.; Zschieschang, U.; Pflaum, J.; Halik, M. Ultralow-Power Organic Complementary Circuits. *Nature* **2007**, *445*, 745–748.

(36) Zhou, L.; Wanga, A.; Wu, S.-C.; Sun, J.; Park, S.; Jackson, T. N. All-Organic Active Matrix Flexible Display. *Appl. Phys. Lett.* **2006**, *88*, 083502.

(37) Meyer zu Heringdorf, F.-J.; Reuter, M. C.; Tromp, R. M. Growth Dynamics of Pentacene Thin Films. *Nature* **2001**, *412*, 517–520.

(38) Ruiz, R.; Nickel, B.; Koch, N.; Feldman, L. C.; Haglund, R. F.; Kahn, A.; Scoles, G. Pentacene Ultrathin Film Formation on Reduced and Oxidized Si Surfaces. *Phys. Rev. B* **2003**, *67*, 125406.

(39) Naito, R.; Toyoshima, S.; Ohashi, T.; Sakurai, T.; Akimoto, K. Molecular Orientation Control of Phthalocyanine Thin Film by Inserting Pentacene Buffer Layer. *Jpn. J. Appl. Phys.* **2008**, *47*, 1416–1418.

(40) Li, F.; Graziosi, P.; Tang, Q.; Zhan, Y.; Liu, X.; Dediu, V.; Fahlman, M. Electronic Structure and Molecular Orientation of Pentacene Thin Films on Ferromagnetic $La_{0.7}Sr_{0.3}MnO_3$. *Phys. Rev. B* **2010**, *81*, 205415.

(41) Kalb, W.; Lang, P.; Mottaghi, M.; Aubin, H.; Horowitz, G.; Wuttig, M. Structure–Performance Relationship in Pentacene/Al_2O_3 Thin-Film Transistors. *Synth. Met.* **2004**, *146*, 279–282.

(42) Ai-Fang, Y.; Qiong, Q.; Peng, J.; Chao, J. Growth Related Carrier Mobility Enhancement of Pentacene Thin-Film Transistors with High-k Oxide Gate Dielectric. *Chin. Phys. Lett.* **2009**, *26*, 078501.

(43) Ruiz, R.; Nickel, B.; Koch, N.; Feldman, L. C.; Haglund, R. F.; Kahn, A.; Family, F.; Scoles, G. Dynamic Scaling, Island Size Distribution, and Morphology in the Aggregation Regime of Submonolayer Pentacene Films. *Phys. Rev. Lett.* **2003**, *91*, 136102.

(44) Campbell, R. B.; Robertson, J. M.; Trotter, J. The Crystal and Molecular Structure of Pentacene. *Acta Crystallogr.* **1961**, *14*, 705–711.

(45) Lanzilotto, V.; Sánchez-Sánchez, C.; Bavdek, G.; Cvetko, D.; Lopez, M. F.; Martin-Gago, J. A.; Floreano, L. Planar Growth of Pentacene on the Dielectric TiO_2 (110) Surface. *J. Phys. Chem. C* **2011**, *115*, 4664–4672.

(46) Albrecht, T. R.; Grütter, P.; Horne, D.; Rugar, D. Frequency Modulation Detection Using High-Q Cantilevers for Enhanced Force Microscope Sensitivity. *J. Appl. Phys.* **1991**, *69*, 668–673.

(47) Sader, J. E.; Sugimoto, Y. Accurate Formula for Conversion of Tunneling Current in Dynamic Atomic Force Spectroscopy. *Appl. Phys. Lett.* **2010**, *97*, 043502.

(48) Lantz, M. A.; Hug, H. J.; Hoffmann, R.; van Schendel, P. J. A.; Kappenberger, P.; Martin, S.; Baratoff, A.; Güntherodt, H.-J. Quantitative Measurement of Short-Range Chemical Bonding Forces. *Science* **2001**, *291*, 2580–2583.

(49) Abe, M.; Sugimoto, Y.; Custance, Ó.; Morita, S. Room-Temperature Reproducible Spatial Force Spectroscopy Using Atom-Tracking Technique. *Appl. Phys. Lett.* **2005**, *87*, 173503.

(50) Sader, J. E.; Jarvis, S. P. Accurate Formulas for Interaction Force and Energy in Frequency Modulation Force Spectroscopy. *Appl. Phys. Lett.* **2004**, *84*, 1801–1803.

(51) Sugimoto, Y.; Pou, P.; Abe, M.; Jelínek, P.; Pérez, R.; Morita, S.; Custance, Ó. Chemical Identification of Individual Surface Atoms by Atomic Force Microscopy. *Nature* **2007**, *446*, 64–67.

(52) Kresse, G.; Furthmüller, J. Efficient Iterative Schemes for Ab Initio Total-Energy Calculations Using a Plane-Wave Basis Set. *Phys. Rev. B* **1996**, *54*, 69993–11186.

(53) Perdew, J. P.; Burke, K.; Ernzerhof, M. Generalized Gradient Approximation Made Simple. *Phys. Rev. Lett.* **1996**, *77*, 3865–3868.

(54) Grimme, S. Semiempirical GGA-Type Density Functional Constructed With a Long-Range Dispersion Correction. *J. Comput. Chem.* **2006**, *27*, 1787–1799.

(55) Aschauer, U.; Chen, J.; Selloni, A. Peroxide and Superoxide States of Adsorbed O_2 on Anatase TiO_2 (101) with Subsurface Defects. *Phys. Chem. Chem. Phys.* **2010**, *12*, 12956.

(56) Cheng, H.; Selloni, A. Energetics and Diffusion of Intrinsic Surface and Subsurface Defects on Anatase TiO_2(101). *J. Chem. Phys* **2009**, *131*, 4703.

Graphical TOC Entry